Cytotoxicity induced by exposure to natural and synthetic tremolite asbestos: An in vitro pilot study

Abstract

Mineral fibers are potential carcinogens to humans. In order to help clarify the etiology of the pathological effects of asbestos, cellular reactions to natural and synthetic asbestos fibers were compared using a lung alveolar cancer cell line (A549 epithelial cells), considered the first target of inhaled micro-environmental contaminants. Natural asbestos tremolite (NAT) fibers were collected from rocks in NW Italy. Synthetic asbestos tremolite (SAT) was iron-free and therefore considered as standard tremolite. Both fibers, subjected to mineralogical characterization by X-ray powder diffractometry, electron microscopy and energy dispersive spectrometry, fell within the definition of respirable and potentially carcinogenic fibers. Several signs of functional and structural cell damage were found after treatment with both fibers, documented by viability, motility, and morphological perturbations. Phalloidin labeling showed irregular distribution of cytoskeletal F-actin, whereas immunohistochemical investigations showed abnormal expression of VEGF, Cdc42, β-catenin, assessed as risks indicators for cancer development. Both fibers caused significant loss of viability, even compared to UICC crocidolite, but, while SAT fibers exerted a more direct cytotoxic effect, survival of damaged cells expressing high VEGF levels was detected after NAT contact. This in vitro pilot study outlines potential health risks of NAT fibers in vivo related to their iron content, which could trigger signaling networks connected with cell proliferation and neoplastic transformation.

Introduction

Asbestos is known to induce lung cancer, malignant mesothelioma and other asbestos-related diseases such as pulmonary interstitial fibrosis (asbestosis) and pleural pathologies in exposed individuals (Mossman and Marsh, 1989, Hansen et al., 1998 and Kamp, 2009). Sites of deposition of asbestos fibers create a favorable environment for development of lung cancers, because in pulmonary lesions proliferating lung fibroblasts may promote proliferation or metaplasia of lung epithelial cells by cell–cell communication and elaboration of growth factors (Mossman et al., 2011).

The term asbestos indicates six hydroxylated inorganic silicate minerals that fall into the serpentine (chrysotile) and the amphibole (asbestos tremolite, actinolite, anthophyllite, grunerite, and crocidolite) mineralogical group based on their crystal structure and chemistry. Their toxicology has been associated with dose, dimension, durability and chemical composition for amphibole asbestos (Mossman et al., 2011). Regarding this last factor, the role of iron is still a subject of debate owing to different investigations made with asbestos containing different amounts of iron (Srivastava et al., 2010).

Asbestos tremolite and actinolite have not been directly used, but they are contained (sometimes with chrysotile) in some kinds of rocks used as construction material for roads, railway beds, ornamental rocks, etc.

Naturally occurring asbestos (NOA) is a term referring to asbestos present in rocks (i.e. asbestos contained in rocks) to distinguish them from asbestos contained in asbestos containing materials (ACM) such as asbestos-cement, as stated by the Agency for Toxic Substances and Disease Registry (http://www.atsdr.cdc.gov/noa/) and by some authors (e.g., Case et al., 2011). In Italy, NOA of tremolite, actinolite and chrysotile are widespread and abundant (as in the Piedmont region, NW Italy) whereas NOA of anthophyllite is less abundant and less common and finally NOA of grunerite, and crocidolite are totally absent (Belluso et al., 1995).

Amphibole fibers were found to be far more potent than chrysotile in causing mesothelioma, a malignant tumor of the pleura or peritoneum, and considerable epidemiological data on tremolite asbestos are related to this form of cancer (McDonald, 2010 and Rudd, 2010). As far as NOA is concerned, in the Upper Susa Valley (Piedmont Region, NW, Italy) where NOA of asbestos tremolite and actinolite abundantly outcrop and are continually excavated, the incidence of pleural and peritoneal malignancies was found to occur frequently in this area (Mirabelli and Cadum, 2002). The natural tremolite asbestos fibers tested in this study come from an area close to the Susa Valley, where specific epidemiological studies have not been reported. Limited data are currently available regarding human exposure to dispersion in air of NOA, therefore risk assessment needs to take into account the effects of weathering on exposure to these fibers (Enrico Favero-Longo et al., 2009).

Characterization of mineral fibers, particularly fibrous amphiboles, which are considered to be more noxious than chrysotile, if not for their biopersistence, is useful both for environmental and for health-related reasons. Besides, the toxicological data obtained investigating fibers of the same asbestos species containing different amounts of iron may improve our understanding of toxicity mechanisms. Given the large number of synthetic and natural fibers and particles introduced into the environment (Donaldson et al., 2010), in vitro screening tests are valuable tools to identify and understand the molecular events that underpin their pathogenicity and to compare the effects exerted by natural and synthetic analogue fibers, with a view to gaining insights into the mechanisms by which these amphibole fibers induce cytotoxicity (Fubini et al., 2010).

This pilot study was devised to determine the mineralogical characterization of natural and synthetic asbestos tremolite (NAT and SAT respectively) by X-ray powder diffractometry (XRPD), transmission and scanning electron microscopy (TEM and SEM), and both with energy-dispersive spectrometry (EDS)

annexed. Moreover, no in vitro data are currently available with regard to these specific fibers, therefore this is the first attempt to estimate the significance of certain metallic cations in the induction of cell alterations. By using in vitro assays it was possible to compare cellular responses to natural fibers (which have a complex chemical composition) with synthetic ones (characterized by a more controlled chemical composition) and help ascertain the role of iron in diseases induced by the asbestos fibers.

The lung cancer cell line A549, a type II alveolar epithelial human line (Lanone et al., 2009), mimics cell–fiber interactions in the lung as they internalize asbestos fibers soon after exposure. The in vitro exposure to asbestos results in mineral fiber uptake with activation of stress signaling and perturbation of several cell function parameters.

A549 cells were used to test the viability and motility, morphological features, cytoskeletal actin organization and the immunohistochemical expression of vascular endothelial growth factor (VEGF), Cdc42, and β-catenin, three molecules involved in cancer development and progression (Pugnaloni et al., 2007 and Pugnaloni et al., 2010). VEGF is a homodimeric glycoprotein with a potent mitogenic effect on endothelial cells (Ferrara and Henzel, 1989) that provides an enhanced ability to establish metastasis at peripheral sites via tumor cell migration through the circulation. Cdc42, a Ras-related GTP-binding protein (Etienne-Manneville and Hall, 2002 and Nakahara et al., 2003), controls the assembly and disassembly of filamentous actin in the cytoskeleton in response to extracellular signals and regulates the formation of membrane projections that are important for forward movement and for dictating cell migration polarity in the early stages of cell spreading. β-Catenin, a component of the Wnt signaling pathway, plays a crucial role as a linker regulating cadherin–actin interactions (Fukumaru et al., 2007 and Herzig et al., 2007).

Material and methods

Minerals

Asbestos tremolite NAT was obtained from serpentine rock collected by one of the authors (E.B.) near Brachiello in Val d'Ala (NW Italian Alps) (Belluso et al., 1995). The SAT fibers were prepared using standard cold-seal hydrothermal techniques (Bloise et al., 2008). The starting materials consisted of silica gel converted to cristobalite by heating at 1400 °C, magnesium oxide (MgO) heated at 900 °C for several hours to eliminate surface hygroscopicity, and calcium oxide (CaO). Synthesis was performed in an externally heated pressure vessel at 780 °C and 1.7 kbar, with a run duration of 120 h. Both samples were gently disaggregated using an agate and pestle mortar in isopropyl alcohol, and then sonicated; this material was deposited onto a copper mesh grid coated with 20 nm carbon film.

An International Union Against Cancer (UICC) crocidolite asbestos sample, used for the cell viability (MTT) assay, had the following physical parameters: 8 × 107 fibers/mg, diameter ratio > 5:1, length > 5 μm, and diameter < 2 μm (Timbrell, 1970 and Unfried et al., 2002).

Characterization of fibers and synthetic materials

The NAT fibers, the starting synthetic materials, and the final SAT product were examined by XRPD using a D5000 diffractometer (Siemens, Germany) equipped with Cu-Ka radiation to identify sample nature, assess the degree of crystallinity, establish whether samples were monophasic, and measure the amount of any associated phases accounting for at least 5% of the volume.

Morphological examination and chemical analysis of tremolite fiber bundles were performed using a Stereoscan 360 SEM (Cambridge, UK) equipped with a Link Pentafet ATW2 (Oxford, UK) analytical EDS system and a Quanta 200 SEM field emission gun (FEG) (FEI, Eindhoven, The Netherlands). Morphology, crystallinity, structural features and chemical composition of single fibers were determined using a CM12 transmission electron microscope (Philips, Eindhoven, the Netherlands) operating at 120 kV, fitted with a LaB6 cathode and a 622 SC 105 camera (Gatan, München, Germany) and equipped with an EDS system (EDAX Si (Li) detector). Unambiguous characterization of individual fibers was achieved by selected area electron diffraction (SAED) and by processing analytical electron microanalysis (AEM) data with an EDAX Genesis 2000 system (Brussels, Belgium) using default K factors.

The UICC crocidolite fibers were used as supplied. NAT and SAT suspensions were prepared with 50 μg of each material per ml of culture medium (equal to 14 μg/cm2) by vortexing at maximum speed for 1 min. In this first approach we used a medium concentration among standards ones (10 and 100 μg/ml) (Cardile et al., 2007 and Musumeci et al., 2011). The dose of fibers used was chosen because it provides good fiber/cell interaction in culture systems and can evoke clearly quantifiable effects among lower and higher doses.

Cell cultures and treatments

The biological effects of NAT and SAT were tested in A549 cells (CCL-185; American Type Culture Collection, Rockville, MD, USA), a human malignant cell line with some features of alveolar epithelial cells. Cells were grown in a controlled atmosphere in RPMI-1640 supplemented with 10% fetal bovine serum (FBS; both from Gibco, Rockville, MD, USA), 2 mM l-glutamine, 100 U/ml penicillin and 100 U/ml streptomycin (Sigma–Aldrich, Milan, Italy). They were passaged every 1–3 days by digestion with 0.25% trypsin (Sigma–Aldrich) containing 0.02% EDTA. After seeding, cells were left to adhere to the substrates for 24 h. The cells were at approximately 70% confluence at the time of exposure to the particles. The spent culture medium was then replaced with the mineral suspensions. All treatments with particles

were performed in RPMI 1640 basal media containing 0.1% FBS. To verify that all the fibers had adhered to the cell surface, 20 drops of medium from each suspension were left standing for 4 h and examined by light microscopy for the presence of any fibers. The same cells, cultured without fibers for 24 h or 48 h, were used as controls.

Cultures and cells treated with crocidolite, NAT, or SAT are described as crocidolite, NAT or SAT cultures or cells. Each experiment was performed three times in triplicate.

Cell viability test (MTT assay)

Cytotoxicity was determined with 3-(4,5-dimethylthiazol-2-yl)-2,5-diphenyltetrazolium bromide (MTT assay) (Lanone et al., 2009) which measures the conversion of MTT to insoluble formazan by dehydrogenase enzymes of the intact mitochondria of living cells. A549 cells were seeded at a density of 3 × 104 cells/well into 24-well microplates. After treatment with the three fiber suspensions, the medium was removed and 200 µl of MTT (Sigma–Aldrich) solution (5 mg/ml in RPM1-1640) plus 1.8 ml RPM1-1640 was added to the plates and incubated for 3 h at 37 °C. The medium was removed and the formazan crystals were dissolved in 2 ml of solvent (4% HCl 1 N in absolute isopropanol). The quantity of crystals formed correlates directly with the number of viable cells. Optical density (OD) was measured at 570 nm (reference filter 690 nm) using a spectrofluorometer (Secomam Anthelie Light, version 3.8, Contardi, Lecco, Italy). Monolayers grown in culture medium without treatment were used as controls and their absorbance values taken as reference. The results were expressed as a proportion of control values (taken as 100%) and their mean ± standard deviation (SD) was used for statistical evaluations. Each experiment was performed three times in triplicate.

Time-lapse video microscopy

For time-lapse video microscopy, A549 cells were seeded in 24-well plates at a density of 1 × 104 cells/cm2 in RPMI-1640 supplemented with 10% FBS and treated a few hours after seeding, to favor adhesion to the substrate. They were then incubated with the NAT or SAT suspension (50 µg/ml medium) for 24 or 48 h; control cultures were not incubated with the suspensions. Subsequently, the fibers were removed with several washes in PBS and the cells incubated in HEPES-modified RPMI-1640 supplemented with 10% FBS, 2 mM l-glutamine, 100 U/ml penicillin, and 100 U/ml streptomycin. For time-lapse recordings, cells were kept at 37 °C and examined in an Eclipse TS-100 inverted microscope (Nikon, Japan) equipped with a 10× objective and a color CCD video camera (JVC TK9 C1381, Japan). Phase-contrast images of living cells were recorded using an AG-TL700 time-lapse VCR (Panasonic, Japan) and digitalized using a video frame grabber card and dedicated software (ImagePro Express, Media Cybernetics, Bethesda, MD, USA). Films of the same fields were made by capturing images every 10 min for up to 24 h. Unattached, round cells and cells dividing during recording intervals were not considered. Diagrams of cell displacement were obtained by processing data with Microsoft Excel, plotting them as x–y diagrams and expressing them as pixel tracks. Migrating cells produced linear tracks, whereas immotile cells were associated with spot-like pixel sequences. Plots were representative of standardized spatial

changes in time (Pugnaloni et al., 2004, Pugnaloni et al., 2007 and Pugnaloni et al., 2010). Each experiment was performed three times in triplicate.

Morphological and histomorphometrical investigations

Pellets were obtained from cell monolayers 24 and 48 h from treatment with the minerals. Untreated cells were used as control cultures. Pellets were obtained by collecting both adherent and floating cells from media of the original cultures. Pellets were fixed in 2% glutaraldehyde in 0.1 M cacodylate buffer (pH 7.4), post-fixed in 1% osmium tetroxide, dehydrated in increasing ethanol concentrations and embedded in Araldite. From each specimen, 20 semi-thin sections were cut at different levels of the pellets, and stained with toluidine blue. Ten fields per section were examined with an Eclipse E600 microscope (Nikon, Italy) at 1000×, using a 100× objective.

Healthy, mitotic, apoptotic and necrotic cells were identified on the basis of the following criteria:

- Healthy cells: spheroid or polygonal shape, central or slightly eccentric nucleus with peripheral heterochromatin, evident nucleoli and distinct, weakly stained cytoplasm.
- Mitotic cells: characteristic arrangement of chromosomes in metaphase or anaphase.
- Apoptotic cells: presence of fragmented and condensed nuclear chromatin clumps on the border of the nuclear envelope; conglomeration of mitochondria, cytoplasm vacuolization and aberrant dyeing with high-affinity staining.
- Necrotic cells: loss of normal cell morphology involving cytoplasm fragmentation, nuclear pyknosis and envelope budding or varying disruption and loss of cellular contents.

Healthy, mitotic, apoptotic and necrotic cells were counted and expressed as proportions of all cells. Morphometrical investigations and statistical evaluations were performed for quantitative assessments by cell counts in 10 fields for each section to a total of 200 counts for specimen. Cells counted were considered representative of almost the entire cell population.

F-actin labeling and immunohistochemical VEGF, β-catenin and Cdc42 detection

Fluorescent phalloidin staining was used to study cytoskeletal filamentous actin. A549 cells were seeded onto two-glass slides at a density of 3.5 × 104 cells/cm2 in RPMI-1640. Cells were treated with NAT or SAT (50 μg/ml) 24 h from seeding and incubated for 24 h or 48 h. They were then washed in PBS, fixed in 4% formaldehyde in PBS for 15 min at 37 °C and permeabilized in 0.5% Triton X-100 buffer for 15 min. After a wash in bovine serum albumin/PBS at 37 °C, a FITC-conjugated phalloidin solution (1:100 dilution in PBS) was added for 30 min at 37 °C. A549 cells cultured without fibers for 24 h or 48 h were used as control. Phalloidin was then removed by washing in PBS and samples were examined using a Nikon Eclipse E600 fluorescence microscope. Ten counts were performed for each slide. Each experiment was

performed three times in triplicate. Values are reported as the percentage of positive cells out of all counted cells and expressed as mean ± SD. Fluorescence intensity was scored as: +− = slight staining; + = moderate staining; ++ = good staining; +++ = strong staining. Staining distribution was described as homogeneous, focal or spotted.

For immunohistochemical labeling cell monolayers were fixed in cold acetone for 10 min, permeabilized in 0.1% Triton X-100 in PBS for 10 min and incubated overnight at 4 °C with anti-VEGF (dil. 1:200), anti-β-catenin (dil. 1:100) and anti-Cdc42 (dil. 1:100; all from Santa Cruz Biotechnology, Santa Cruz, CA, USA) monoclonal antibodies. They were then immunostained using the streptavidin–biotin peroxidase technique (LSAB peroxidase kit, Dako Cytomation, Milan, Italy). After incubation with 0.05% 3,3′-diaminobenzidine (Sigma–Aldrich, Milan, Italy) in 0.05 M Tris buffer, pH 7.6 with 0.01% hydrogen peroxide, sections were counterstained with Mayer's hematoxylin (Bio-Optica, Milan, Italy), dehydrated in ethanol and coverslipped with Eukitt mounting medium (Electron Microscopy Sciences, PA, USA). Positive controls for antibody against VEGF, β-catenin and Cdc42 were represented by A549 cells treated with asbestiform antigorite, previously shown to react with primary antibodies (Pugnaloni et al., 2010). For negative controls primary antibody was replaced with non-immune serum. Each experiment was performed three times in triplicate.

The number of F-actin, VEGF, Cdc42 and β-catenin positive cells was evaluated by quantitative immunoassays (Taylor and Levenson, 2006). All counts were performed simultaneously by two investigators blinded to the treatment (G.L. and A.P.), using a double-headed light microscope. Both had to agree on the count of cell positivity. Images were captured with a Nikon DS-Vi1 digital camera (Nikon Instruments, Europe BV, Kingston, Surrey, England) and NIS Elements BR 3.22 imaging software (Nikon Instruments, Europe BV, Kingston, Surrey, England) was used. Counts were performed in 10 fields/sample (field: 0.07 mm2, magnification: 400×) and quantified as a percentage of the total counted cells. The fields were randomly selected evaluating the most positive, moderate and less positive areas.

Staining intensity was assessed using a four-point scoring system: +− = slight staining; + = moderate staining; ++ = good staining; +++ = strong staining.

Statistical analysis

All data were obtained in triplicate from three independent experiments and expressed as mean ± SD. Significance was determined by one-way analysis of variance followed by the t-test with Bonferroni's correction for multiple comparisons (Primer of biostatistics, 6th ed. S.A. Glantz, McGraw-Hill, Milan, Italy). A p-value of less than 0.05 was considered statistically significant.

Results

Natural asbestos tremolite (NAT)

The SEM examinations (Fig. 1a) disclosed aggregates of long, rigid fibers whose diameter ranged from 1 to 1.5 μm, and thicker fiber bundles measuring 150–200 μm in diameter. The XRPD investigations showed high crystallinity and the absence, at this scale, of other mineral phases. TEM and SAED examination of single fibers showed high crystallinity, absence of structural defects (again at this scale) and a fiber axis running in the [0 0 1] direction, the latter feature being consistent with the amphibole structure of the mineral. NAT fibers appeared stiff, with diameters ranging from 1 to 1.5 μm; a few thicker crystals ranged in diameter from 15 to 20 μm and therefore a greater amount of fibers fell within the definition of respirable and potentially carcinogenic fibers (Stanton et al., 1981 and Suzuki et al., 2005) and they do not show characteristics of cleavage fragments, i.e. they are not shorter than 10 μm and have not a diameter less than 1 μm (Addison and McConnell, 2008).

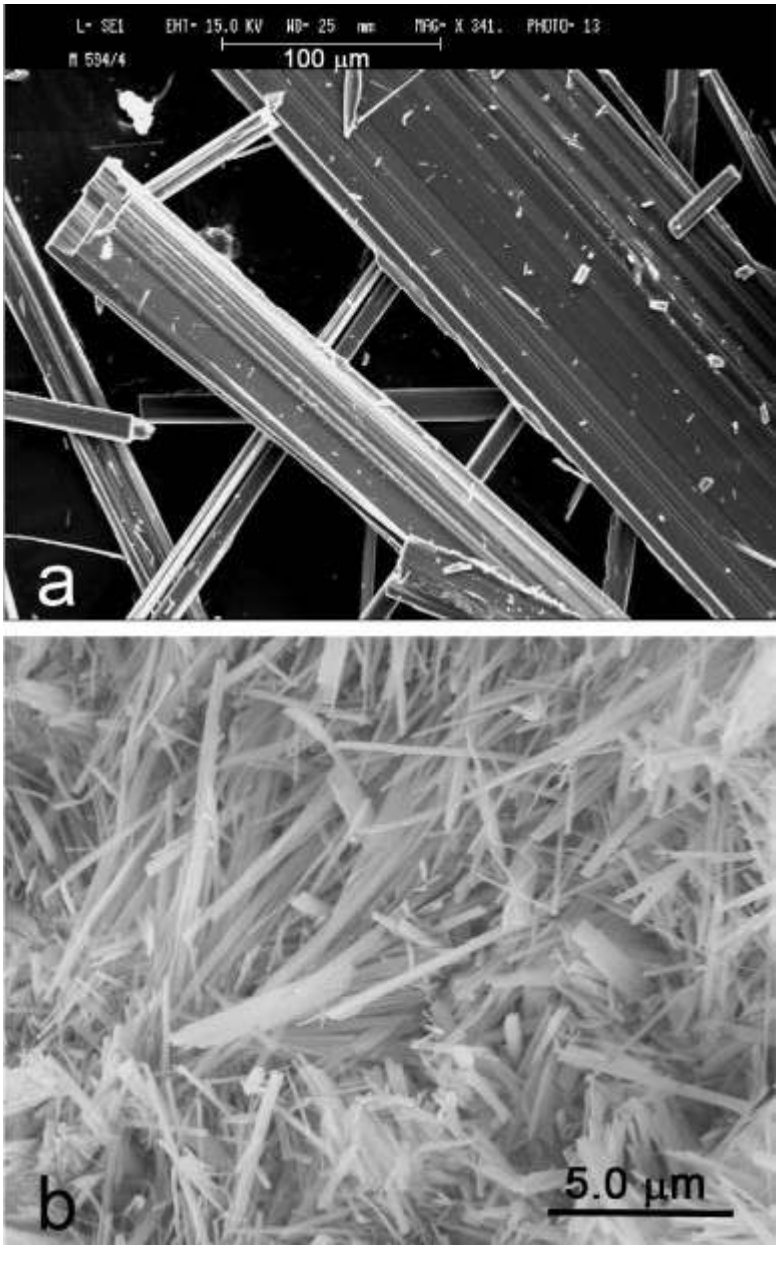

Fig. 1.

(a) Secondary electron SEM image of natural asbestos tremolite (NAT) and (b) secondary electron SEM image of synthetic asbestos tremolite (SAT).

High-resolution TEM (HRTEM) showed talc lamellae developing on the edge of some fibers. AEM analysis of various fibers documented a homogeneous chemical composition. The crystallochemical formula of NAT fibers was Ca1.66(Mg4.62Fe2+0.27Al0.18Mn0.02)Σ5.09Si8.00O22(OH)2, consistent with the theoretical formula of tremolite Ca2(Mg,Fe2+)5[Si8O22](OH)2.

Synthetic asbestos tremolite (SAT)

SAT displayed very high crystallinity on XRPD (Bloise et al., 2008). Traces of quartz were also noted. SEM (Fig. 1b) and conventional TEM (CTEM) (Fig. 2a and b) observations showed thin, rigid fibers with an average length of 10 µm. Their diameter ranged from 0.04 to 0.68 µm (average: 0.13 µm), fibers measuring < 0.25 µm accounting for 94% of all fibers. From the dimensional point of view, all the fibers fell in the category of either respirable or potentially carcinogenic fibers and they did not appear as cleavage fragments (Addison and McConnell, 2008). The SAED patterns (Fig. 2c) showed that the individual fibers exhibited high crystallinity, but also structural defects consisting of planar faults (chain width defects) (Bozhilov et al., 2007) which were clearly displayed on HRTEM. The semi-quantitative chemical composition of several fibers, as determined by AEM analysis, showed complete absence of impurities related to the synthesis process. Their crystallochemical formula was $Ca_{1.71}Mg_{5.24}Si_{8.01}O_{22}(OH)_2$. Intergrown polysomatic slabs were seen in line with previous reports by various researchers.

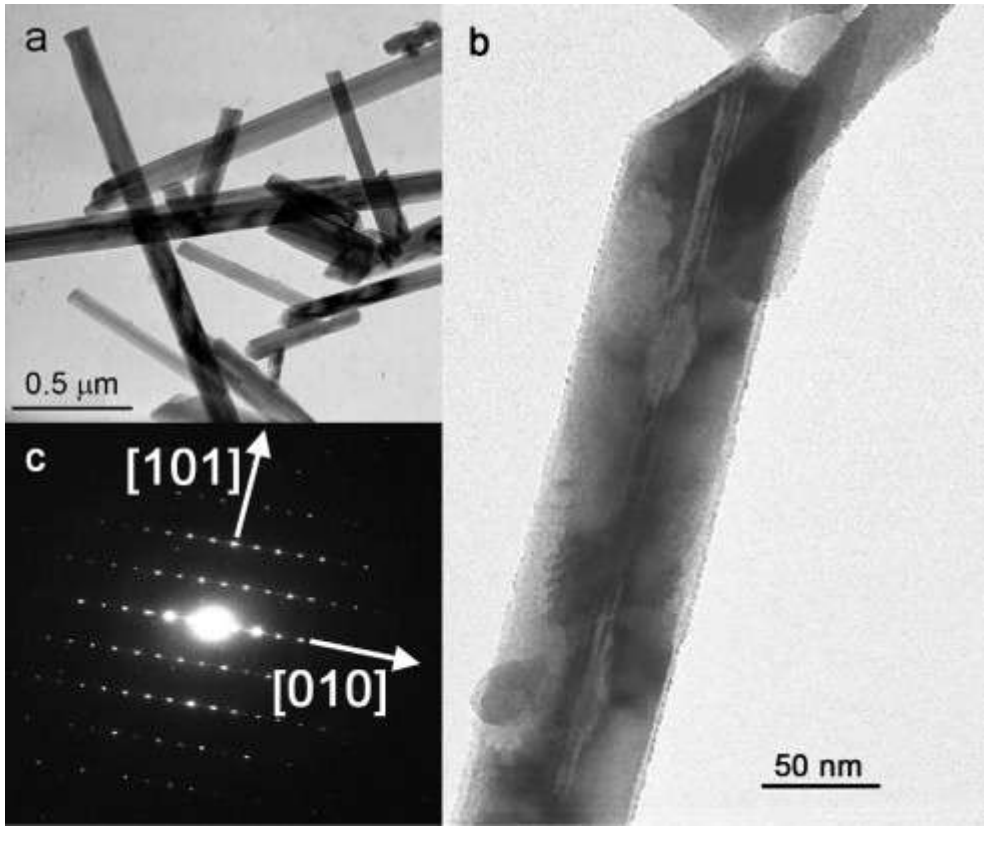

Fig. 2.

(a) CTEM image of several SAT fibres; (b) high magnification and (c) SAED pattern of a single SAT fibre.

From our mineralogical studies it was estimated that the total superficial areas of SAT fibers was about 10 times higher with respect to the NAT total superficial areas, in a ratio almost equal to 1 NAT/100 SAT fibers per cm2.

Cell viability (MTT assay)

The MTT assay (Fig. 3) showed that cell viability decreased in treated cells compared with controls (taken to represent 100%). At 24 h 66.8%, 42.3%, and 64%, respectively, of the cells treated with NAT, SAT or crocidolite were viable. At 48 h the viable cells fell to 21.4%, 10.2% and 53%, respectively. Significant differences in cell viability were observed in both treated cells with respect to the controls and between NAT and SAT treated cells at both time points.

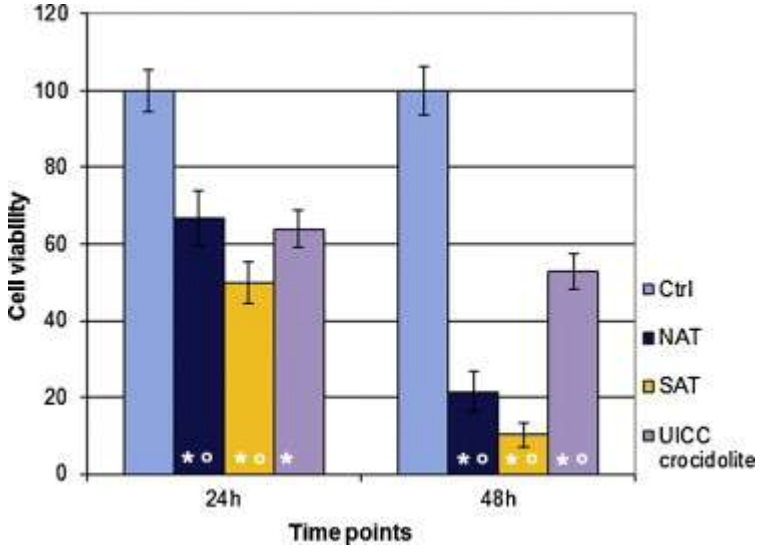

Fig. 3.

A549 cell viability measured by the MTT assay in control cultures and cultures exposed to natural tremolite (NAT), synthetic tremolite (SAT) and UICC crocidolite for 24 and 48 h. Mean ± SD. The values of the optical density were measured at λ = 570 nm and expressed as percentage with respect to the optical density of the controls. Untreated control cells were considered as 100% of cell viability. Significant differences ($p < 0.05$) were observed in treated cells with respect to the controls (*); between NAT and SAT treatments (°) at 24 h; among all treatments at 48 h (°).

Morphological and histomorphometrical investigations

The results of the morphological and histomorphometrical investigations are shown in Fig. 4 and Table 1, respectively. The control cultures, examined at 70% confluence, appeared to be mainly composed of adhering cells with a polygonal shape and often contained mitotic elements. At 24 h cells formed nests and chains that were better organized at 48 h. Necrotic and apoptotic cells were seen at 24 h and increased at 48 h, owing to cell crowding. After treatment with NAT and SAT, chains were no longer detected and the viable cells were isolated, surrounded by necrotic elements and cell debris. Healthy, mitotic, apoptotic and necrotic cell features were significantly different in treated and control specimens.

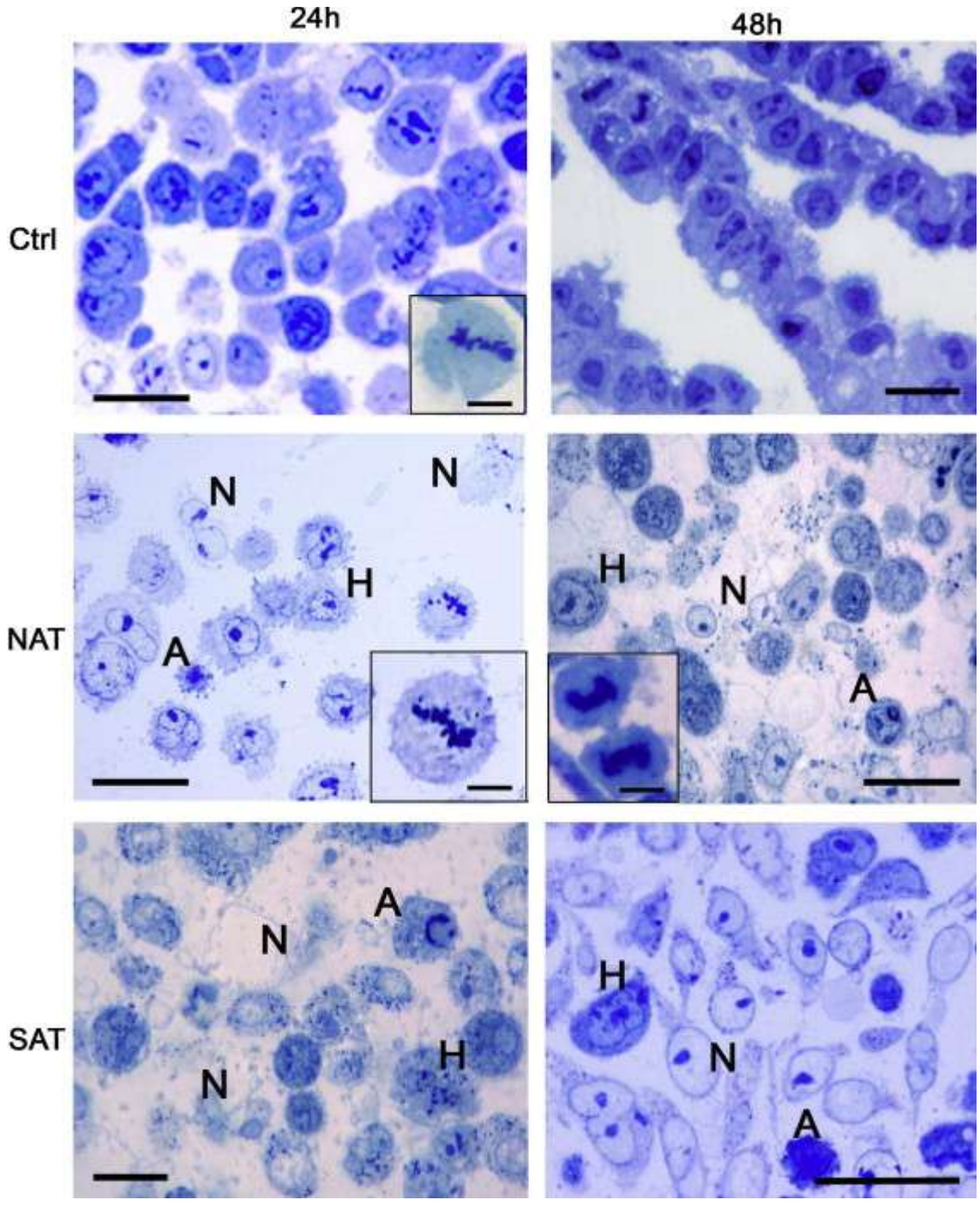

Fig. 4.

Toluidine blue staining. Semi-thin sections of control and NAT- and SAT-treated A549 cells at 24 and 48 h. Polygonal spread cells and sporadic mitotic elements (insert) were detected in control cultures; cellular nests and chains were more frequent at 48 h. Treated cultures showed few healthy isolated cells (H) and larger amounts of necrotic cells (N) at both time points with both fiber types. Apoptotic cells (A) were also detected. In NAT cultures mitotic cells were found at 24 and 48 h; mitotic cells were also detected

(insets). The SAT cultures prevalently contained necrotic and apoptotic cells. Scale bars = 12 µm; inserts = 5 µm.

Table 1.

Proportion of healthy, mitotic, apoptotic and necrotic cells in A549 cultures treated with NAT or SAT (mean ± SD): morphometric evaluations in semithin sections.

A549 cells	**Healthy cells (%)**	**Mitotic cells (%)**	**Apoptotic cells (%)**	**Necrotic cells (%)**
24 h				
1. Ctrl	90 ± 1.99	5.7 ± 0.8	1.5 ± 0.4	2.2 ± 2.1
2. NAT	56 ± 2.5	2.7 ± 0.1	3.10 ± 0.5	36.2 ± 2.6
3. SAT	42.31 ± 1.9	0.7 ± 0.1	2.1 ± 0.6	55.43 ± 5.1
	1 *vs* 2	1 *vs* 3	2 *vs* 1	2 *vs* 1
Bonferroni's *t*-test $p < 0.05$	1 *vs* 3	1 *vs* 2	3 *vs* 1	2 *vs* 3
	3 *vs* 2	2 *vs* 3		3 *vs* 1
48 h				
1. Ctrl	89 ± 2.5	2.7 ± 0.2	2.3 ± 0.2	6.04 ± 1.2
2. NAT	42 ± 1.7	0.2 ± 0.1	8.54 ± 0.6	49.4 ± 2.2
3. SAT	33.5 ± 3.8	0	4.34 ± 0.9	62.3 ± 6.2
	1 *vs* 2	1 *vs* 3	2 *vs* 1	3 *vs* 1
Bonferroni's *t*-test $p < 0.05$	1 *vs* 3	1 *vs* 2	2 *vs* 3	2 *vs* 3
	3 *vs* 2		3 *vs* 1	2 *vs* 1

Ctrl, control; NAT, natural asbestos tremolite; SAT, synthetic asbestos tremolite.

After NAT and SAT treatment the proportion of healthy cells decreased significantly and that of necrotic cells increased significantly compared with the control cultures and between treatments at both time points, with broader variations after SAT exposure. The proportion of mitotic cells decreased significantly after both treatments, but especially after SAT, compared with control cultures at 24 and 48 h, and compared with NAT cells at 24 h. Apoptotic cells increased after treatment, to a greater extent after NAT exposure. Significantly different proportions of healthy, mitotic and necrotic cells were observed between NAT and SAT cultures at 24 h. At 48 h mitotic cells were not significantly different and apoptotic cells increased more in NAT-treated specimens.

Time-lapse video microscopy

Time-lapse video microscopy was used to study the effects of NAT and SAT fibers on the motility of individual cells, as cell migratory capacity of live adherent cells was monitored. Control, NAT and SAT cultures were monitored for up to 48 h (Fig. 5). NAT and SAT cultures showed adherent survived cells with loss of motility seen 24 h after treatment, with greater reductions at 48 h.

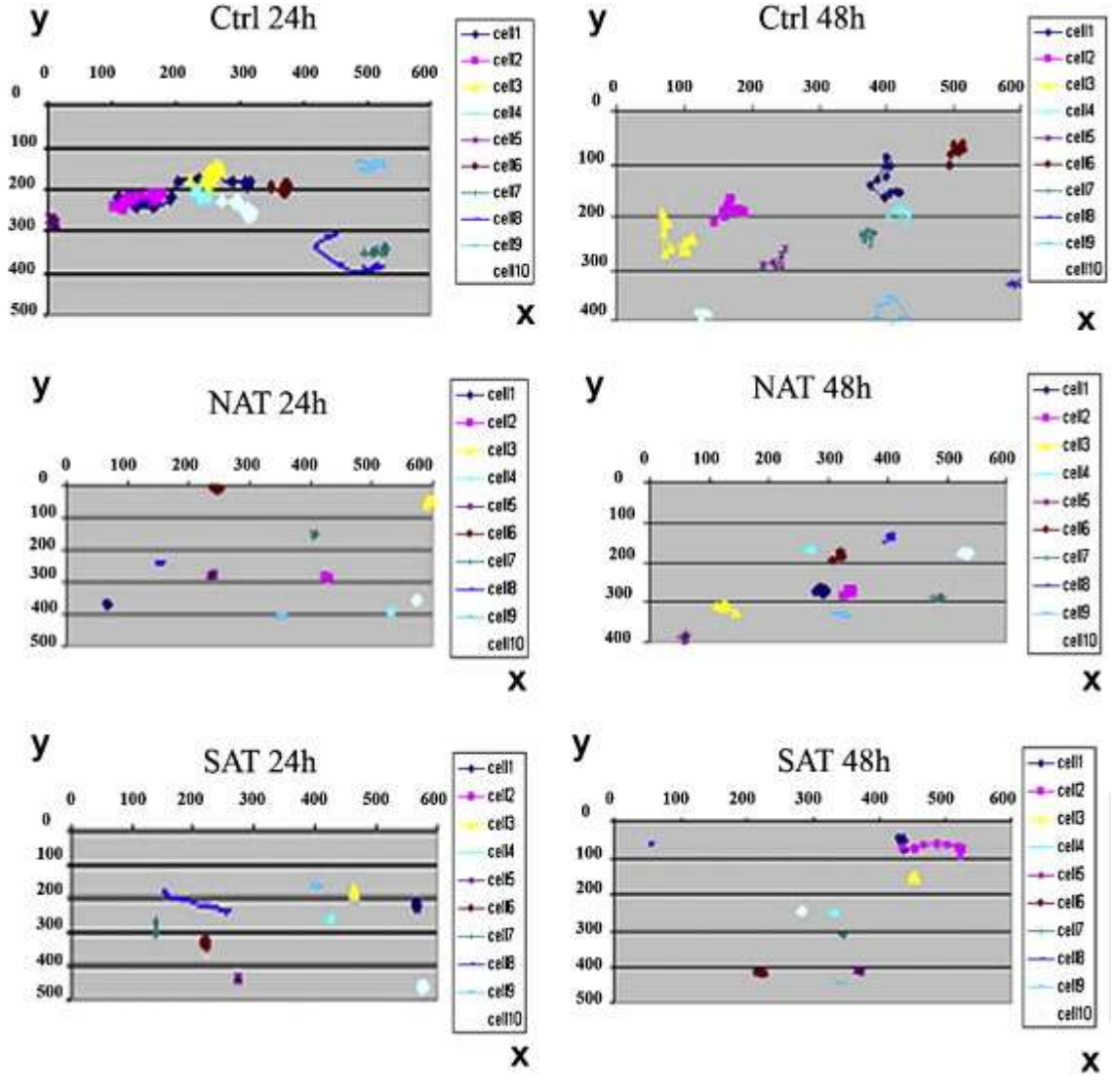

Fig. 5.

Time-lapse video microscopy recordings of control and NAT- and SAT-treated A549 cells at 24 h and 48 h. Loss of cell motility is clearly evident in treated cultures.

F-actin staining

In the control culture, phalloidin staining yielded good fluorescence, depicting the organization of F-actin filaments at 24 and 48 h. Cortical F-actin was associated with the inner face of the plasma membrane (good/strong intensity); the cytoskeletal network exhibited a homogeneous cytoplasmic distribution and good/strong intensity at 24 h and strong intensity at 48 h (Fig. 6 and Table 2).

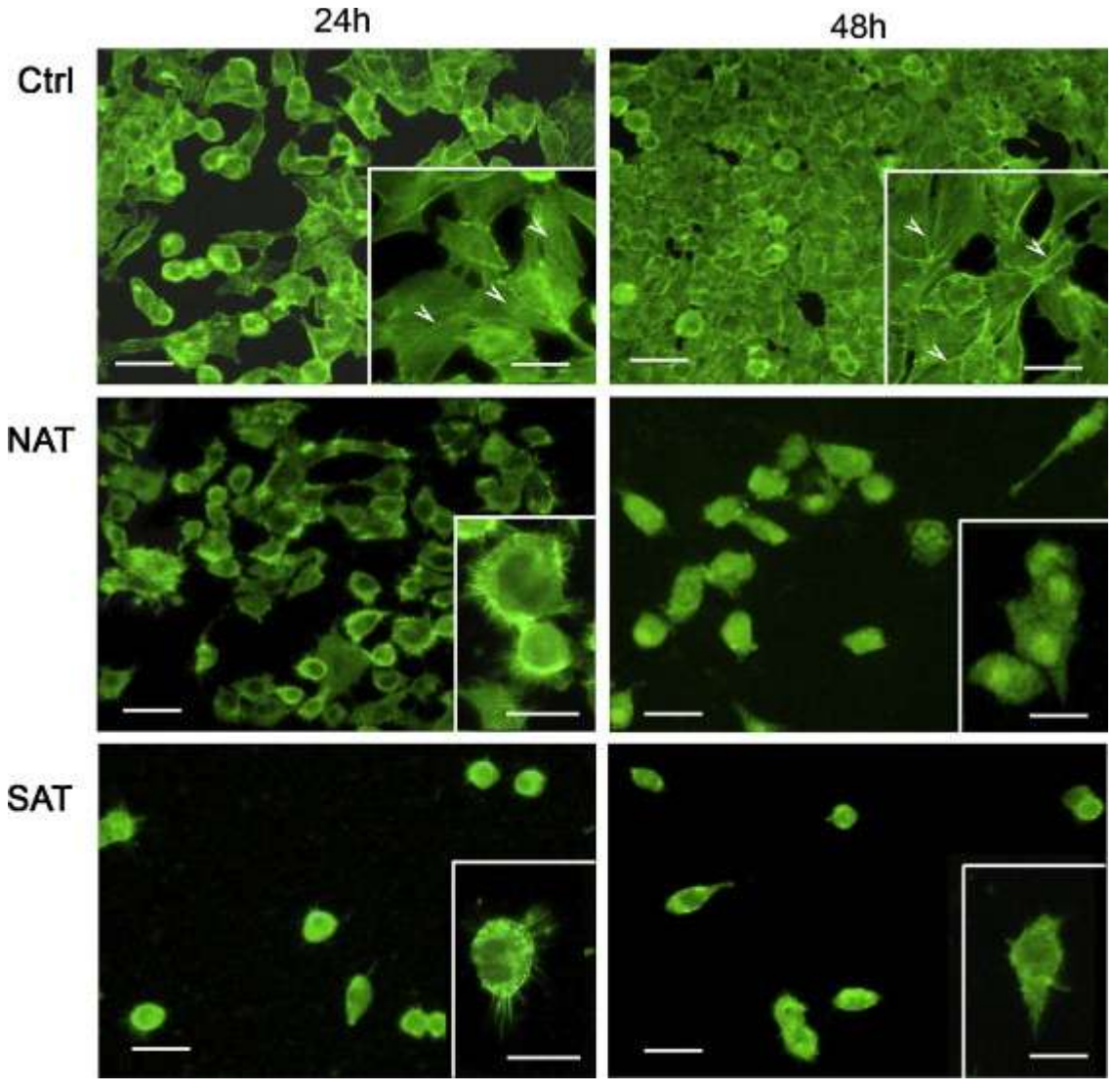

Fig. 6.

Fluorescence imaging of phalloidin staining for detection of F-actin at 24 h and 48 h. Control A549 cultures at 24 h and 48 h showing filamentous cytoskeletal actin (arrowheads). In NAT and SAT cells actin staining was irregular in the cytoplasm, with a more granular signal than in control cultures and a focal and spotted distribution. Insets: cells from the same cultures as Ctrl, NAT and SAT at higher magnification. Scale bars = 20 μm; inserts = 10 μm.

Table 2.

Fluorescence phalloidin staining for F-actin localization.

	Membrane		Cytoplasm	
A549 cells				
	% of positive cells	**Intensity score**	**% of positive cells**	**Intensity score**
24 h				
1 Ctrl	90 ± 5.04	++/+++	95 ± 10.41	+++
2 NAT	80 ± 15.21	++/+++ focal	90 ± 5.32	++
3 SAT	75 ± 10.16	++ spotted	90 ± 2.35	++
Bonferroni's *t*-test $p < 0.05$	n.s.		n.s.	
48 h				
1 Ctrl	95 ± 5.20	++/+++	90 ± 5.34	++/+++
2 NAT	8 ± 5.74	+−	15 ± 4.23	+
3 SAT	50 ± 10.03	++ spotted	50 ± 10.41	++
Bonferroni's *t*-test $p < 0.05$	1 *vs* 2		1 *vs* 2	
	1 *vs* 3		1 *vs* 3	
	2 *vs* 3		2 *vs* 3	

Ctrl, control; NAT, natural asbestos tremolite; SAT, synthetic asbestos tremolite. Proportion of positive cells (mean ± SD). n.s., not significant. Intensity score, fluorescence intensity in positive cells. +− = slight; + = moderate; ++ = good; +++ = strong.

In treated cells, actin was no longer detected as cytoskeletal filaments but it appeared irregularly structured with spotted (granular) staining and focal distribution.

In NAT cells at 24 h no significant differences were found in the proportions of cells showing plasma membrane or cytoplasmic staining compared with the control culture. Plasma membrane staining intensity was good to strong, often focal; cytoplasmic staining was good. SAT cells at 24 h showed good, spotted staining both of the plasma membrane and the cytoplasm on 75% and 90% of cells, respectively.

Differences in the number of cells showing membrane and/or cytoplasmic staining between treated and control cells were not significant. In NAT cells at 48 h phalloidin staining of cell membranes was slight in intensity and found in a very low proportion of positive cells (8%). Only 15% of cells showed moderate cytoplasmic staining. In SAT cells at 48 h 50% of positive cells showed good staining intensity and spotted membrane staining, while the other 50% showed no membrane staining and only good cytoplasmic staining. Differences in the number of cells showing membrane and/or cytoplasmic staining between treated and control cells were significant.

Immunohistochemical VEGF, β-catenin and Cdc42 detection

The results of immunohistochemical staining are shown in Fig. 7 (24 h) as well as in Fig. 8 (48 h) and Table 3. In our in vitro system VEGF showed cytoplasmic staining; Cdc42 was generally detected in perinuclear cytoplasm and often in cytoplasmic sprouts. β-Catenin that in normal conditions is localized at membrane level was also detected in the cytoplasm of A549 cells. The proportion of positive cells and the staining intensity of NAT and SAT cells at 24 and 48 h were significantly different compared with the respective controls.

- 24 h: Control cultures exhibited moderate VEGF expression in 63% of positive cells. VEGF expression was increased in NAT and SAT cells compared with control cultures both in terms of number of positive cells and of staining intensity; the latter was stronger in NAT cells. Cdc42 staining was weak and was seen in 80% of control cells. The proportion of positive cells and staining intensity decreased after both treatments. β-Catenin was detected in the cytoplasm of 80% of control cells (moderate or good intensity) and on the cell membrane in 60% of cells (good staining). Cytoplasmic expression and staining intensity decreased significantly after both treatments. Cell membrane expression and staining intensity decreased significantly after NAT treatment and in particular after SAT treatment it could be no longer be detected.
- 48 h: Control cells showed moderate-good VEGF expression in 75% of positive cells. Strong Cdc42 expression was seen in nearly all control cells. Moderate cytoplasmic expression of β-catenin was noted in 30% of control cells; membrane expression was strong in 70% of control cells. NAT treatment was associated with an increased proportion of VEGF-positive cells and strong staining. In SAT cells increments were less marked. Cdc42 expression exhibited the same trend as at 24 h, with decreased proportions of positive cells with respect to control cultures. The cells expressing β-catenin in the cytoplasm increased after NAT treatment compared with control cells. β-Catenin expression at the cell membrane level showed the same trend as at 24 h.

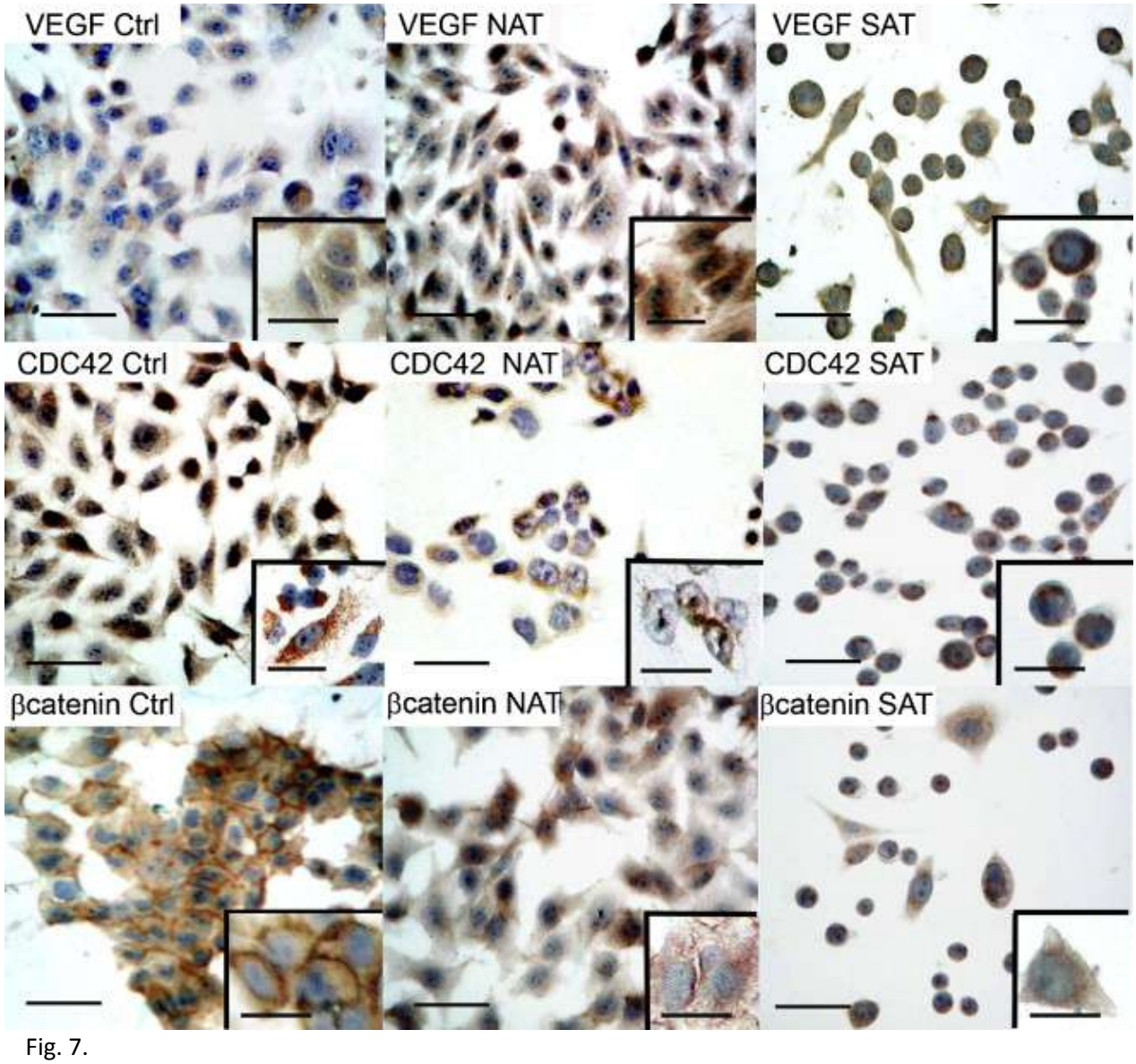

Fig. 7.

Immunohistochemical expression of VEGF, Cdc42 and β-catenin in control and treated cultures at 24 h. VEGF and Cdc42 showed cytoplasmic staining. VEGF expression was increased in NAT and SAT cells both in terms of number of positive cells and of staining intensity. Cdc42 staining was weak and the proportion of positive cells and staining intensity decreased after both treatments. β-Catenin was detected in the cytoplasm and on the cell membrane in control cells. Cytoplasmic expression and staining intensity decreased significantly after both treatments; in particular after SAT treatment cell membrane expression was no longer detected (scale bars = 25 μm). Inserts: higher magnification of the labeled cells (scale bars = 10 μm).

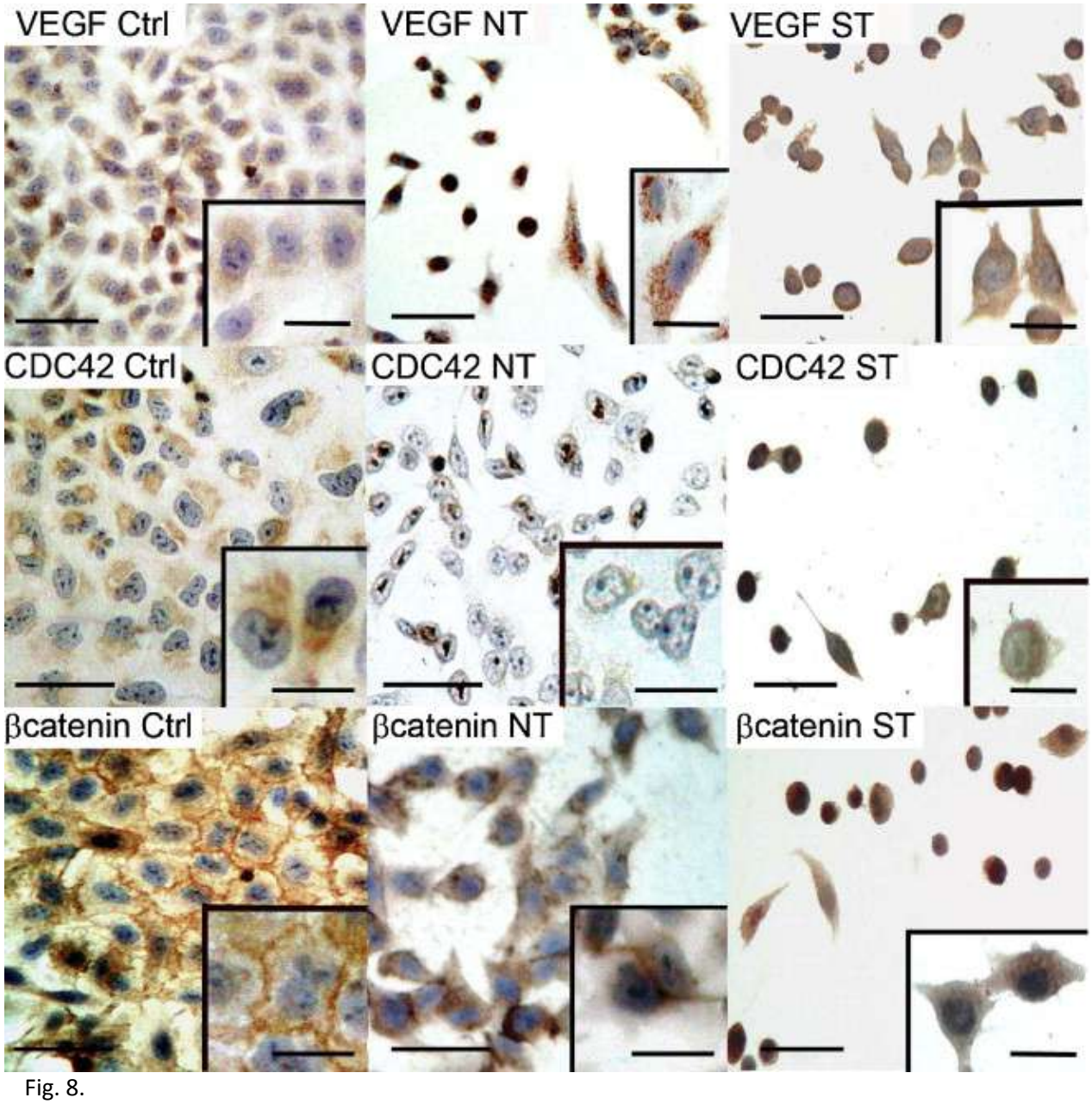

Fig. 8.

Immunohistochemical expression of VEGF, Cdc42 and β-catenin in control and treated cultures at 48 h. VEGF and Cdc42 expression showed the same trend as at 24 h. β-Catenin expression increased in the cytoplasm after NAT treatment, while after SAT exposure the expression on cell membrane showed the same trend as at 24 h (scale bars = 25 μm). Inserts: higher magnification of the labeled cells (scale bars = 10 μm).

Table 3.

Immunohistochemical expression of VEGF, Cdc42 and β-catenin.

	VEGF		**Cdc42**		**β-Catenin**			
A549 cells					**Cytoplasm**		**Membrane**	
	% of positive cells	**Intensity score**	**% of positive cells**	**Intensity score**	**% of positive cells**	**Intensity score**	**% of positive cells**	**Intensity score**
24 h								
1. Ctrl	63 ± 4.3	+	80 ± 7.65	+	80 ± 9.05	+/++	60 ± 5.25	++
2. NAT	91 ± 5.05	+++	35 ± 11.05	+–	30 ± 7.0	+–	40 ± 4.5	+
3. SAT	78 ± 3.2	++	30 ± 8.05	+–	30 ± 9.00	+	0	–
Bonferroni's *t*-test,$p < 0.05$	1 *vs* 2 1 *vs* 3 2 *vs* 3		1 *vs* 3 1 *vs* 2		1 *vs* 3 1 *vs* 2		1 *vs* 3 1 *vs* 2 2 *vs* 3	
48 h								
1. Ctrl	75 ± 4.4	+/++	95 ± 3.5	+++	30 ± 5.20	+	70 ± 4.25	+++
2. NAT	90 ± 5.7	+++	15 ± 8.8	+–	50 ± 7.6	+	25 ± 12.5	+/++
3. SAT	81 ± 4.3	++	20 ± 11.4	+	20 ± 10.0	+	0	–
Bonferroni's *t*-test,$p < 0.05$	1 *vs* 2		1 *vs* 2 1 *vs* 3		2 *vs* 3		1 *vs* 3 1 *vs* 2 2 *vs* 3	

Ctrl, control; NAT, natural asbestos tremolite; SAT, synthetic asbestos tremolite. Proportion of positive cells (mean ± SD); n.s., not significant. Intensity score, staining intensity in positive cells. +– = slight; + = moderate; ++ = good; +++ = strong.

Discussion

Tremolite is a mineral of the amphibole family with fibers that consist of prismatic crystals with a chain-like appearance, as directed by the crystal structure. Its commercial use has been less extensive than that of chrysotile, amosite, and crocidolite. Amosite, tremolite and chrysotile fibers have been found in most lungs of miners with heavy mixed exposure to amphiboles and chrysotile (Churg, 1988 and Churg and Vedal, 1994). The tremolite fibers could be important in the pathogenesis of lung tumors, since greater relative amounts of tremolite were found in patients with mesothelioma.

The aim of this study was to characterize the natural tremolite from the Western Italian Alps and the iron free synthetic analogue asbestos fibers and to compare in vitro their cytotoxic effects by functional, morphological and immunohistochemical assays on A549 cells, a non-small cell lung carcinoma (NSCLC)-derived cell line mimicking the human lung environment, used in a number of toxicological assays (Lanone et al., 2009, Msiska et al., 2010 and Musumeci et al., 2011).

Our findings indicate that both fiber types affected the in vitro system with different intensity. The MTT assay showed significantly reduced cell viability already at 24 h. At both time points the strongest cytotoxic effects were exerted by SAT, even compared with UICC crocidolite. These functional effects agreed with the morphometrical data from semi-thin sections, which documented significantly greater amounts of necrotic cells in the SAT cultures. The higher amounts of healthy cells and mitotic figures found at 24 and 48 h in the NAT cultures reflect a less toxic effect of the natural fibers and suggest a preserved proliferative potential in some surviving cells. NAT exposure induced a significant increase also in apoptotic cells, especially at 48 h. This finding is sustained by the data of the MTT test, which assays the mitochondrial enzyme status. Apoptosis requires energy in mammalian cells, where mitochondria are key regulators of the intrinsic death pathway activated by asbestos (Upadhyay and Kamp, 2003).

Examination of the time-lapse video microscopy data demonstrated that NAT and SAT treatment also affected cell motility at both time points. This functional perturbation was reflected in the cell structure as shown by F-actin staining, which showed that the proportions of cells exhibiting membrane or cytoplasm positivity at 24 h were not significantly different from those seen in control cells. The focal fluorescent staining seen in NAT cells could be related to an irregular organization of the cytoskeletal filamentous network associated with the cell membrane. Actin organization was more strongly affected

by SAT treatment and exhibited a less intense, spotted staining, due to irregularly structured intracellular F-actin, causing impaired cell function. In eukaryotic cells, actin filaments work as force-generating structural scaffolds (Goley and Welch, 2006) playing important roles in several vital processes, including cell migration, endocytosis, vesicle trafficking and cytokinesis (Ridley, 2001).

Abnormal expressions of VEGF, Cdc42 and β-catenin in NAT and SAT cells were demonstrated by immunohistochemical investigations. VEGF is regarded as an important factor sustaining cell invasion and metastasis, released as a consequence of inflammation or tumorigenesis in injured tissues, where it is mitogenic to vascular endothelial cells and sustains tumor angiogenesis (Hillegass et al., 2010). It has also been demonstrated that asbestos contact causes an increase in VEGF expression in humans (Amati et al., 2008) and VEGF-related tumor angiogenesis (Bremnes et al., 2006). The increased VEGF expression found in vitro after NAT treatment may be considered as a strong risk factor related particularly to the natural fibers, as shown by the large proportions of positive cells and strong staining noted in NAT cultures at both time points.

Cdc42, one of the best characterized Rho family members, plays a key role in cytoskeletal actin organization, thus affecting many cellular processes including migration, vesicle trafficking, proliferation and cell polarity (Heasman and Ridley, 2008). Its inactivation or down-regulation may be involved in aberrant cancer cell polarity within the epithelial cell lining that causes cancer cell invasion into the surrounding environment (Yao et al., 2002 and Zhang et al., 2008). Cdc42 is normally expressed in human tumor cell lines, where, together with β-catenin and filamentous actin, it regulates cell–cell and cell–matrix adhesion, influences the motile properties of tumor cells in vitro and the metastatic ability of lung cancer cells in vivo (Nakashima and Lazo, 2010). β-Catenin normally localizes to adherens junctions in A549 cells, but accumulates intracellularly as a result of the removal of adhesion molecules from membranes no longer engaged in formation of cell–cell contacts. In our in vitro system, loss of cell junctions in NAT and SAT cultures was associated with decreased expression of Cdc42 and membrane β-catenin that may destabilize cell connections and enhance cell migration and metastasis.

Phagocytic cells that engulf asbestos fibers produce large amounts of free radicals due to their inability to digest the fibers. Cytotoxic and genotoxic effects exerted by asbestos fibers are further sustained by their content in iron ions which induce generation of reactive oxygen species and/or reactive nitrogen species (Mossman and Marsh, 1989, Srivastava et al., 2010 and Mossman et al., 2011) causing mitochondrial damage, impaired cell motility (Okayasu et al., 1999 and Bergamini et al., 2007), apoptotic induction (Srivastava et al., 2010) and risk of tumor progression (Luanpitpong et al., 2010) according to epidemiological studies indicating that iron-containing asbestos fibers appear more carcinogenic (Toyokuni, 2009). Iron ions that were found in NAT fibers (Rinaudo et al., 2004) might contribute to the overall toxicity as in the case of an iron-rich tremolite sample from Lanzo Valley (Italian Western Alps) (Turci et al., 2009). SAT is a well defined compound coming from laboratory synthesis and characterized by smaller fibers providing a larger contact surface with cells that is easier for uptake. As postulated by

some authors (Dogan et al., 2008) for erionite, the microstructures of asbestos minerals draw attention to surface area or surface-area-to-volume ratio concepts and their relationship to the pulmonary diseases caused by the mineral. Lower NAT cytotoxicity can be related to its greater fiber dimensions providing a reduced surface area. NAT fibers might be taken up with more difficulty by the cells in an in vitro system.

Cells that survived NAT treatment at 24 h were isolated, apparently healthy and still engaged in mitotic activity, despite the irregular organization of their cytoskeletal actin. The data obtained so far in cultures exposed to the medium dose (50 µg/ml) suggest that while SAT seems to induce morpho-functional modifications with more direct cytotoxic aspects via necrotic processes, NAT might exert a toxic effect with a higher risk of cell transformation after in vivo exposure. It is tempting to speculate that when in vivo exposure to mineral fibers is insufficient to trigger immediate necrosis, oxidative and non-oxidative pathogenic mechanisms may lead to a selection of cellular clones characterized by progressive derangement towards abnormal transformation. The dose of fibers used was chosen because it can clearly evoke quantifiable effects between lower and higher doses. In the future we intend to treat primary lung and mesothelial cells with different doses of fibers under all the experimental conditions.

Our study sustains the concept that mineralogical characterization is an important tool for relating toxicological characteristics with composition of inorganic fibers. Morpho-functional perturbations observed in this study, compare the different effects of respirable natural and synthetic asbestos fibers and highlight the risk of in vivo NAT exposure for workers and the potential danger to people living in the vicinity of tremolite outcrops.

The well-characterized SAT fibers can be used as standard mineral fibers in future investigations for achieving a better understanding of asbestos toxicity mechanisms and the role of iron in asbestos-induced disease. The studies carried out to date show that in vitro investigations of synthetic asbestos, because of their controlled chemical composition, are of medical as well as social interest and can help predict the in vivo risks associated with natural tremolite and possible different compositions (Wagner et al., 1982 and Davis et al., 1991).

The results of this pilot study however, coupled with the ban on the use of asbestos in Italy (Law 257/929), demonstrate the need for further research on natural asbestos, and alternative fibers as safer substitutive materials.

References

Addison and McConnell, 2008

J. Addison, E.E. McConnell

A review of carcinogenicity studies of asbestos and nonasbestos tremolite and other amphiboles

Regul Toxicol Pharmacol, 52 (2008), pp. S187–S199

Amati et al., 2008

M. Amati, M. Tomasetti, L. Mariotti, L.M. Tarquini, M. Valentino, L. Santarelli

Assessment of biomarkers in asbestos-exposed workers as indicators of cancer risk

Mutat Res, 655 (2008), pp. 52–58

Belluso et al., 1995

E. Belluso, R. Compagnoni, G. Ferraris

Occurrence of asbestiform minerals in the serpentinites of the Piemonte Zone, Western Alps

Giornata di studio in ricordo del Prof. Stefano Zucchetti, Politecnico di Torino (1995), pp. 57–64

Bergamini et al., 2007

C. Bergamini, R. Fato, G. Biagini, A. Pugnaloni, F. Giantomassi, E. Foresti et al.

Mitochondrial changes induced by natural and synthetic asbestos fibers: studies on isolated mitochondria

Cell Mol Biol (Noisy-le-grand), 52 (Suppl.) (2007), pp. OL905–OL913

Bloise et al., 2008

A. Bloise, E. Fornero, E. Belluso, E. Barrese, C. Rinaudo

Synthesis and characterization of tremolite asbestos fibres

Eur J Mineral, 20 (2008), pp. 1027–1033

Bozhilov et al., 2007

K.N. Bozhilov, D. Brownstein, D.M. Jenkins

Biopyribole evolution during tremolite synthesis from dolomite and quartz in CO2–H2O fluid

Am Mineral, 92 (2007), pp. 898–908

Bremnes et al., 2006

R.M. Bremnes, C. Camps, R. Sirera

Angiogenesis in non-small cell lung cancer: the prognostic impact of neoangiogenesis and the cytokines VEGF and bFGF in tumours and blood

Lung Cancer, 51 (2006), pp. 143–158

Cardile et al., 2007

V. Cardile, L. Lombardo, E. Belluso, A. Panico, M. Renis, A. Gianfagna et al.

Fluoro-edenite fibers induce expression of Hsp70 and inflammatory response

Int J Environ Res Public Health, 4 (2007), pp. 195–202

Case et al., 2011

W.B. Case1, J.L. Abraham, G. Meeker, F.D. Pooley, K.E. Pinkerton

Applying definitions of “asbestos” to environmental and “low-dose” exposure levels and health effects, particularly malignant mesothelioma

J Toxicol Environ Health B, 14 (2011), pp. 3–39

Churg, 1988

A. Churg

Chrysotile, tremolite, and malignant mesothelioma in man

Chest, 93 (1988), pp. 621–628

Churg and Vedal, 1994

A. Churg, S. Vedal

Fiber burden and patterns of asbestos-related disease in workers with heavy mixed amosite and chrysotile exposure

Am J Respir Crit Care Med, 150 (1994), pp. 663–669

Davis et al., 1991

J.M. Davis, J. Addison, C. McIntosh, B.G. Miller, K. Niven

Variations in the carcinogenicity of tremolite dust samples of differing morphology

Ann N Y Acad Sci, 643 (1991), pp. 473–490

Dogan et al., 2008

A.U. Dogan, M. Dogan, J.A. Hoskins

Erionite series minerals: mineralogical and carcinogenic properties

Environ Geochem Health, 30 (2008), pp. 367–381

Donaldson et al., 2010

K. Donaldson, F.A. Murphy, R. Duffin, C.A. Poland

Asbestos, carbon nanotubes and the pleural mesothelium: a review of the hypothesis regarding the role of long fibre retention in the parietal pleura, inflammation and mesothelioma

Part Fibre Toxicol, 22 (2010), pp. 7–19

Enrico Favero-Longo et al., 2009

S. Enrico Favero-Longo, F. Turci, M. Tomatis, R. Compagnoni, R. Piervittori, B. Fubini

The effect of weathering on ecopersistence, reactivity, and potential toxicity of naturally occurring asbestos and asbestiform minerals

J Toxicol Environ Health A, 72 (2009), pp. 305–314

Etienne-Manneville and Hall, 2002

S. Etienne-Manneville, A. Hall

Rho GTPases in cell biology

Nature, 420 (6916) (2002), pp. 629–635

Ferrara and Henzel, 1989

N. Ferrara, W.J. Henzel

Pituitary follicular cells secrete a novel heparin-binding growth factor specific for vascular endothelial cells

Biochem Biophys Res Commun, 161 (1989), pp. 851–858

Fubini et al., 2010

B. Fubini, M. Ghiazza, I. Fenoglio

Physico-chemical features of engineered nanoparticles relevant to their toxicity

Nanotoxicology, 4 (2010), pp. 347–363

Fukumaru et al., 2007

K. Fukumaru, N. Yoshii, T. Kanzaki, T. Kanekura

Immunohistochemical comparison of beta-catenin expression by human normal epidermis and epidermal tumors

J Dermatol, 34 (2007), pp. 746–753

Goley and Welch, 2006

E.D. Goley, M.D. Welch

The ARP2/3 complex: an actin nucleator comes of age

Nat Rev Mol Cell Biol, 7 (2006), pp. 13–26

Hansen et al., 1998

J. Hansen, N.H. de Klerk, A.W. Musk, M.S.T. Hobbs

Environmental exposure to crocidolite and mesothelioma. Exposure–response relationships

Am J Respir Crit Care Med, 157 (1998), pp. 69–75

Heasman and Ridley, 2008

S.J. Heasman, A.J. Ridley

Mammalian Rho GTPases: new insights into their functions from in vivo studies

Nat Rev Mol Cell Biol, 9 (2008), pp. 690–701

Herzig et al., 2007

M. Herzig, F. Savarese, M. Novatchkova, H. Semb, G. Christofori

Tumor progression induced by the loss of E-cadherin independent of beta-catenin/Tcf-mediated Wnt signaling

Oncogene, 26 (2007), pp. 2290–2298

Hillegass et al., 2010

J.M. Hillegass, A. Shukla, M.B. MacPherson, J.P. Bond, C. Steele, B.T. Mossman

Utilization of gene profiling and proteomics to determine mineral pathogenicity in a human mesothelial cell line (LP9/TERT-1)

J Toxicol Environ Health A, 73 (2010), pp. 423–436

Kamp, 2009

D.W. Kamp

Asbestos-induced lung diseases: an update

Transl Res, 153 (2009), pp. 143–152

Lanone et al., 2009

S. Lanone, F. Rogerieux, J. Geys, A. Dupont, E. Maillot-Marechal, J. Boczkowski et al.

Comparative toxicity of 24 manufactured nanoparticles in human alveolar epithelial and macrophage cell lines

Part Fibre Toxicol, 30 (2009), pp. 6–14

Luanpitpong et al., 2010

S. Luanpitpong, S.J. Talbott, Y. Rojanasakul, U. Nimmannit, V. Pongrakhananon, L. Wang et al.

Regulation of lung cancer cell migration and invasion by reactive oxygen species and Caveolin-1

J Biol Chem, 285 (2010), pp. 38832–38840

McDonald, 2010

J.C. McDonald

Epidemiology of malignant mesothelioma – an outline

Ann Occup Hyg, 54 (2010), pp. 851–857

Mirabelli and Cadum, 2002

D. Mirabelli, E. Cadum

Mortality among patients with pleural and peritoneal tumors in Alta Valle di Susa

Epidemiol Prev, 26 (2002), pp. 284–286

Msiska et al., 2010

Z. Msiska, M. Pacurari, A. Mishra, S.S. Leonard, V. Castranova, V. Vallyathan

DNA double-strand breaks by asbestos, silica, and titanium dioxide. Possible biomarker of carcinogenic potential?

Am J Respir Cell Mol Biol, 43 (2010), pp. 210–219

Mossman and Marsh, 1989

B.T. Mossman, J.P. Marsh

Evidence supporting a role for active oxygen species in asbestos induced toxicity and lung disease

Environ Health Perspect, 81 (1989), pp. 91–94

Mossman et al., 2011

B.T. Mossman, M. Lippmann, T.W. Hesterberg, K.T. Kelsey, A. Barchowsky, J.C. Bonner

Pulmonary endpoints (lung carcinomas and asbestosis) following inhalation exposure to asbestos

J Toxicol Environ Health B, 14 (2011), pp. 76–121

Musumeci et al., 2011

G. Musumeci, V. Cardile, C. Fenga, S. Caggia, C. Loreto

Mineral fibre toxicity: expression of retinoblastoma (Rb) and phosphor retinoblastoma (pRb) protein in alveolar epithelial and mesothelial cell lines exposed to fluoro-edenite fibres

Cell Biol Toxicol, 27 (2011), pp. 217–225

Nakahara et al., 2003

H. Nakahara, T. Otani, T. Sasaki, Y. Miura, Y. Takai, M. Kogo

Involvement of Cdc42 and Rac small G proteins in invadopodia formation of RPMI7951 cells

Genes Cells, 8 (2003), pp. 1019–1027

Nakashima and Lazo, 2010

M. Nakashima, J.S. Lazo

Phosphatase of regenerating liver-1 promotes cell migration and invasion and regulates filamentous actin dynamics

J Pharmacol Exp Ther, 334 (2010), pp. 627–633

Okayasu et al., 1999

R. Okayasu, L. Wu, T.K. Hei

Biological effects of naturally occurring and man-made fibres: in vitro cytotoxicity and mutagenesis in mammalian cells

Br J Cancer, 79 (1999), pp. 1319–1324

Pugnaloni et al., 2004

A. Pugnaloni, F. Giantomassi, T. Armeni, M. Serresi, G. Principato, F. Fazioli et al.

In vitro H2O2 stress and patterns of mitochondrial damage in the NCTC 2544 continuous cell line – a morphologic and morphometric study

Cell Mol Biol (Noisy-le-grand), 50 (2004), pp. OL517–OL526

Pugnaloni et al., 2007

A. Pugnaloni, G. Lucarini, F. Giantomassi, L. Lombardo, S. Capella, E. Belluso et al.

In vitro study of biofunctional indicators after exposure to asbestos-like fluoro-edenite fibres

Cell Mol Biol (Noisy-le-grand), 7 (2007), pp. OL965–OL980

Pugnaloni et al., 2010

A. Pugnaloni, F. Giantomassi, G. Lucarini, S. Capella, M.M. Belmonte, M. Orciani et al.

Effects of asbestiform antigorite on human alveolar epithelial A549 cells: a morphological and immunohistochemical study

Acta Histochem, 112 (2010), pp. 133–146

Ridley, 2001

A. Ridley

Rho Proteins: linking signaling with membrane trafficking

Traffic, 2 (2001), pp. 303–310

Rinaudo et al., 2004

C. Rinaudo, E. Belluso, D. Gastaldi

Assessment of the use of Raman spectroscopy for the determination of amphibole asbestos

Mineral Mag, 68 (2004), pp. 455–465

Rudd, 2010

R.M. Rudd

Malignant mesothelioma

Br Med Bull, 93 (2010), pp. 105–123

Srivastava et al., 2010

R.K. Srivastava, M. Lohani, A.B. Pant, Q. Rahman

Cyto-genotoxicity of amphibole asbestos fibers in cultured human lung epithelial cell line: role of surface iron

Toxicol Ind Health, 26 (2010), pp. 575–582

Stanton et al., 1981

M.F. Stanton, M. Layard, A. Tegeris, E. Miller, M. May, E. Morgan et al.

Relation of particle dimension to carcinogenicity in amphibole asbestoses and other fibrous minerals

J Natl Cancer Inst, 67 (1981), pp. 965–975

Suzuki et al., 2005

Y. Suzuki, S.R. Yuen, R. Ashley

Short, thin asbestos fibers contribute to the development of human malignant mesothelioma: pathological evidence

Int J Hyg Environ Health, 208 (2005), pp. 201–210

Taylor and Levenson, 2006

C.R. Taylor, R.M. Levenson

Quantification of immunohistochemistry – issues concerning methods, utility and semiquantitative assessment II

Histopathology, 49 (2006), pp. 411–424

Timbrell, 1970

V. Timbrell

Characteristics of the International Union Against Cancer standard reference samples of asbestos

H.A. Shapiro (Ed.), Pneumoconiosis, Proceedings of the International Conference, Johannesburg, Cape Town, South Africa, Oxford University Press, Oxford (1970), pp. 28–36

Toyokuni, 2009

S. Toyokuni

Mechanisms of asbestos-induced carcinogenesis

Nagoya J Med Sci, 71 (2009), pp. 1–10

Turci et al., 2009

F. Turci, M. Tomatis, R. Compagnoni, B. Fubini

Role of associated mineral fibres in chrysotile asbestos health effects: the case of balangeroite

Ann Occup Hyg, 53 (2009), pp. 491–497

Unfried et al., 2002

K. Unfried, C. Schürkes, J. Abel

Distinct spectrum of mutations induced by crocidolite asbestos: clue for 8-hydroxydeoxyguanosine-dependent mutagenesis in vivo

Cancer Res, 62 (2002), pp. 99–104

Upadhyay and Kamp, 2003

D. Upadhyay, D.W. Kamp

Asbestos-induced pulmonary toxicity: role of DNA damage and apoptosis

Exp Biol Med (Maywood), 228 (2003), pp. 650–659

Wagner et al., 1982

J.C. Wagner, M. Chamberlain, R.C. Brown, G. Berry, F.D. Pooley, R. Davies et al.

Biological effects of tremolite

Br J Cancer, 45 (1982), pp. 352–360

Yao et al., 2002

R. Yao, Y. Wang, R.A. Lubet, M. You

Differentially expressed genes associated with mouse lung tumor progression

Oncogene, 21 (2002), pp. 5814–5821

Zhang et al., 2008

S. Zhang, K. Schafer-Hales, F.R. Khuri, W. Zhou, P.M. Vertino, A.I. Marcus

The tumor suppressor LKB1 regulates lung cancer cell polarity by mediating cdc42 recruitment and activity

Cancer Res, 68 (2008), pp. 740–748